FRONTIERS OF PHYSICS

RESEARCH ARTICLE
Volume 17 / Issue 6 / 63507 / 2022

$P2_12_12_1$-C16: An ultrawide bandgap and ultrahard carbon allotrope with the bandgap larger than diamond

Mingqing Liao[1,†], Jumahan Maimaitimusha[1], Xueting Zhang[1], Jingchuan Zhu[2], Fengjiang Wang[1,‡]

1 School of Materials Science and Engineering, Jiangsu University of Science and Technology, Zhenjiang 212003, China
2 School of Materials Science and Engineering, Harbin Institute of Technology, Harbin 150001, China
Corresponding authors. E-mail: †mingqing_liao@just.edu.cn, ‡fjwang@just.edu.cn
Received April 25, 2022; accepted August 18, 2022

ABSTRACT

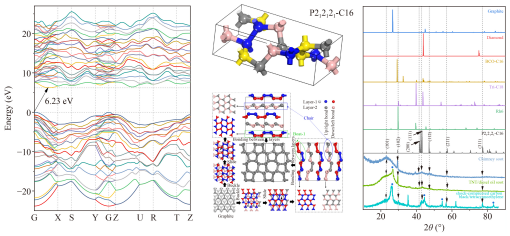

Ultrawide bandgap semiconductor, e.g., diamond, is considered as the next generation of semiconductor. Here, a new orthorhombic carbon allotrope ($P2_12_12_1$-C16) with ultrawide bandgap and ultra-large hardness is identified. The stability of the newly designed carbon is confirmed by the energy, phonon spectrum, ab-initio molecular dynamics and elastic constants. The hardness ranges from 88 GPa to 93 GPa according to different models, which is comparable to diamond. The indirect bandgap reaches 6.23 eV, which is obviously larger than that of diamond, and makes it a promising ultra-wide bandgap semiconductor. Importantly, the experimental possibility is confirmed by comparing the simulated X-ray diffraction with experimental results, and two hypothetical transformation paths to synthesize it from graphite are proposed.

Keywords carbon allotrope, ultrawide bandgap semiconductor, ultrahard, first-principles

1 Introduction

Wide bandgap (WBG) semiconductors work well at higher temperatures, voltages, and present higher switching speeds than traditional Si-based semiconductors [1], which makes the WBG semiconductor a promising candidate for extreme environments applications. Currently, the development of WBG materials is mainly focused on SiC, GaN [2, 3], of which the bandgaps are 3.2 eV and 3.4 eV, respectively. With the increase of bandgap, many of the figures-of-merit for device performance is more than linear with bandgap [4]. For example, the Baliga figure of merit (BFOM) [5] improves about 34 times if the bandgap increase from 3.4 to 6.0 [4]. Hence, it is necessary to design ultrawide bandgap (UWBG) semiconductors with bandgap >3.4 eV [4].

On the other hand, benefiting from the various bonding types of carbon, as well as design tools (such as RG^2 [6] and CALYPSO [7]), plenty of interesting carbon allotropes are found in both experiments and theoretical calculations [8, 9], such as fullerene [10], carbon nanotube [11], graphene [12], paracrystalline diamond [13], and T-carbon [14]. Among those carbon allotropes, there are many UWBG allotropes emerged: diamond (5.47 eV [15]), T5-carbon (4.30 eV) [16], $P222_1$-C8 (4.75 eV) [17], BC14 (5.64 V) [18], HSH-carbon (4.8 eV) [19] and so on. However, the bandgap larger than diamond is quite rare in the carbon allotropes.

Recently, several UWBG carbon allotropes with bandgap larger than diamond are designed. Lv *et al.* [20] proposed a new carbon allotrope (tri-C18) with bandgap of 6.32 eV based on the particle swarm optimization. Several previous allotropes are recognized as UWBG materials in He *et al.*'s work [21], e.g., the superdense carbon tP12 [22], I-4 [23], W-carbon [24]. In addition, they designed several new large bandgap semiconductors, including I-43d and Pbam-32 by using the ab initio

https://doi.org/10.1007/s11467-022-1204-z

random structure search (AIRSS) [25] and random sampling strategy combined with space group and graph theory (RG^2) [6]. Among those UWBG allotropes, the I-43d presents the largest bandgap in the known carbon allotropes, reaching 7.24 eV (Note: Clathrate-VIII presents 7.3 eV bandgap predicted in Ref. [26], however it obviously overestimate the bandgap of diamond, we still take I-43d as the largest bandgap carbon allotrope). However, the simulated X-ray diffraction (XRD) of I-43d is not shown in previous experiments and no potential transformation path from graphite or carbon nanotube is found [21].

In the present work, we predict a new ultrahard UWBG semiconductor by RG^2, naming $P2_12_12_1$-C16. The bandgap is predicted to be 6.23 eV, and the hardness is about 90 GPa. Moreover, the simulated XRD shows that the main peaks in $P2_12_12_1$-C16 match well with previous experiments, and the hypothetical transition pathways from graphite are given.

2 Computational methods

The new structure is generated by specifying the space group using RG^2 software [6], which has been successfully applied to discover some novel carbon allotropes [21, 27]. The CASTEP software is used to execute the first-principles calculations [28]. The HSE06 [29] hybrid functional is used to calculate the band structures and GGA-PBE [30] for other properties. The on-the-fly generated (OTFG) norm-conserving pseudopotential [31] with energy cut-off of 720 eV is used in the phonon and electronic band structure calculation, and the OTFG ultra-soft pseudopotential [32] with energy cut-off of 440 eV for other calculations. The k-points are generated by specifying the separation of 0.07 $Å^{-1}$ to ensure accuracy. The relaxation is done by Broyden-Fletcher-Goldfarb-Shanno (BFGS) algorithm [33]. The convergence criteria of relaxation are 5×10^{-6} eV/atom in energy, 0.01 eV/Å in residual force per atom, 5×10^{-4} Å in max displacement, and 0.02 GPa in max stress. The phonon spectrum is calculated using density functional perturbation theory (DFPT) [34]. *Ab-initio* molecular dynamics (AIMD) are performed for 5000 steps with 1 fs/step at 273 K and 1000 K using the NVT ensemble, and $2 \times 2 \times 2$ supercell is used in AIMD. The second- (SOECs) and third- (TOECs) order elastic constants are calculated using the strain-stress method [35] implemented in Elastic3rd [36], and the strain range used is –6% to 6% with a strain-step of 1%. The fifth-order terms are taken into consideration to eliminate the higher-order effect [37]. The polycrystalline elastic modulus is evaluated by Voigt-Reuss-Hill (VRH) approximation [38] implemented in the ElasticPOST code [39].

3 Results and discussion

3.1 Structure characteristics

The structure of $P2_12_12_1$-C16 is shown in Fig. 1. The crystal is orthorhombic with a $P2_12_12_1$ (No.19) space group, and the lattice constants are $a = 4.3246$ Å, $b = 2.4974$ Å, and $c = 8.5030$ Å, respectively. There are 16 atoms in the unit cell, which can be divided into 4 inequivalent Wyckoff positions: 4*a* (0.3446, 0.4348, 0.0419) (C1, pink in Fig. 1), 4*a* (0.0801, 0.1865, 0.2843) (C2, yellow in Fig. 1), 4*a* (0.9796, 0.5661, 0.0389) (C3, grey in Fig. 1) and 4*a* (0.4102, 0.3054, 0.2235) (C4, blue in Fig. 1). All the bonds in $P2_12_12_1$-C16 are sp^3-hybridized and 8 different kinds of bonds exist in the unit cell. The bond length in $P2_12_12_1$-C16 ranges from 1.540 Å to 1.606 Å, and the average value is 1.558 Å, which is slightly larger than that of diamond (about 1.547 Å). Using the bonds information, the hardness of $P2_12_12_1$-C16 can be evaluated by Gao's model [40] as 91.2 GPa. The density of $P2_12_12_1$-C16 is 3.475 g/cm^3, which is slightly smaller than that of diamond.

To identity the uniqueness in carbon allotrope, the topology of $P2_12_12_1$-C16 is analyzed by topcryst.com [41] to be 4,4,4,4T39648-HZ, which only presents the same underlying net with a kind of silica reported in Deem's Hypozeolites database [42], and there is no redundancy with ICSD or Samara Carbon Allotrope Database (SACADA) [43], as well as a recently high-throughput computational work [44]. To display the topology more clearly, the natural tiling [45] is calculated by ToposPro [41] and Gavrog code (http://gavrog.org) [46], and the result is shown in Fig. 2. $P2_12_12_1$-C16 contains four different natural tiling, including two $[6{\cdot}7^2]$ (one 6-ring and two 7-rings, hereinafter), $[5^2{\cdot}6^4]$ and $[6^2{\cdot}7^2]$.

3.2 Stability

The energy-volume curve of $P2_12_12_1$-C16 is shown in Fig. 3(a) and compared with some recently proposed carbon allotropes. Obviously, $P2_12_12_1$-C16 is a metastable carbon allotrope, and at equilibrium, the energy of $P2_12_12_1$-C16 is about 0.304 eV higher than that of diamond. Though the energy of $P2_12_12_1$-C16 is slightly

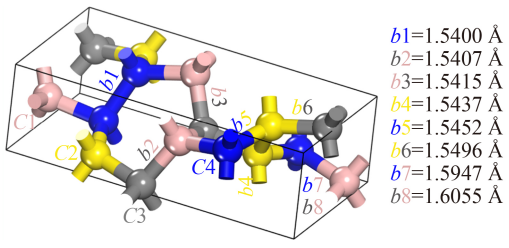

Fig. 1 Structure characteristics of $P2_12_12_1$-C16.

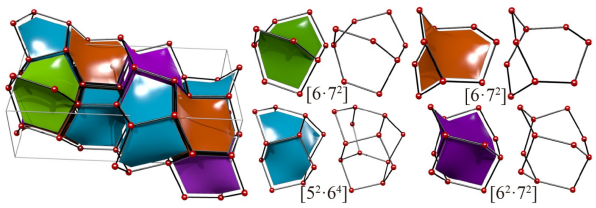

Fig. 2 Topology analysis by natural tiling.

higher than that of Tri-C18 [20] and BCO-C16 [47], the energy is apparently lower than that of PCB [48], BC8 [49], BC12 [50], T5-Carbon [16], T-Carbon [14] and Rh6 [51]. From Fig. 3(b), the energy of $P2_12_12_1$-C16 is almost parallel to that of diamond when pressure is applied to the structure, while the relative energy (to diamond) of the other allotropes, such as graphite, Tri-C18, BCO-C16, and Rh6, is increased with pressure. Hence, the $P2_12_12_1$-C16 is more stable than BCO-C16, graphite, and tri-C18 when the pressure is larger than 3GPa, 33GPa, and 55GPa, respectively, indicating that $P2_12_12_1$-C16 is promising to be synthesized by graphite at high pressure.

Besides the energetical stability, the dynamical stability is confirmed by the phonon spectrum, as shown in Fig. 3(c). The largest frequency in $P2_12_12_1$-C16 is about 38.5 THz (~40 THz for diamond), indicating the strongest bond strength in $P2_12_12_1$-C16 is comparable with diamond. In addition, the peak of phonon DOS appears at the region of high-frequency, indicating there is a large number of strong bonds in $P2_12_12_1$-C16. The AIMD is performed to check the thermal stability and the results are shown in Fig. 3(d) and Fig. 3(e). The topology of the structure keeps the same with the initial structure after 5ps at both 273 K and 1000 K, which confirms the thermal stability of $P2_12_12_1$-C16.

3.3 Mechanical properties

To estimate the mechanical stability of $P2_12_12_1$-C16, the SOECs and TOECs are calculated and shown in Table 1. For orthorhombic crystal, the Born stability conditions can be expressed as: $C_{11}>0$, $C_{44}>0$, $C_{55}>0$, $C_{66}>0$, $C_{11}C_{22}>C_{12}^2$ and $C_{11}C_{22}C_{33} + 2C_{12}C_{13}C_{23} - C_{11}C_{23}^2 - C_{22}C_{13}^2 - C_{33}C_{12}^2>0$ [52]. Obviously, $P2_12_12_1$-C16 is mechanically stable. Using the single-crystal elastic constants, the 3D distribution of polycrystalline elastic modulus is illustrated in Fig. 4. The maximum of B, E, and G occurs in the [010] direction, while the minimum value occurs in the xz plane for B, [101] directions for E, and [100] direction for G. The averaged value of B, G, and E in $P2_12_12_1$-C16 is slightly smaller than that of diamond. The B/G of $P2_12_12_1$-C16 is about 0.85, which is slightly larger than that of diamond (0.83), indicating that $P2_12_12_1$-C16 is brittle but tougher than diamond according to Pugh's criteria [53]. The hardness of $P2_12_12_1$-C16 evaluated according to the empirical formula based on the elastic modulus is 88.0 GPa (Chen's model [54]), 89.2 GPa (Tian's model [55]), and 92.7 GPa (Efim's model [56]). Both the elastic-modulus-

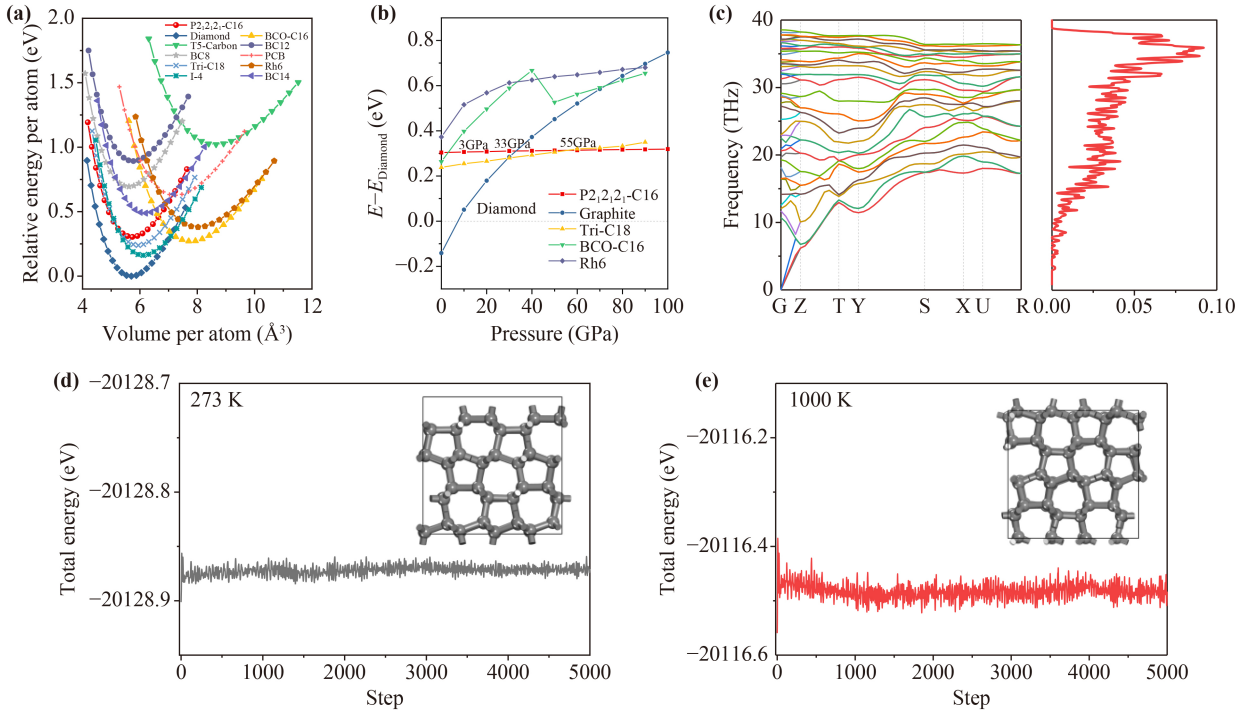

Fig. 3 Stability of $P2_12_12_1$-C16. **(a)** Energy-volume curve; **(b)** Relative energy as a function of pressure; **(c)** Phonon band structure and density of state (DOS); **(d)** Energy evolution of AIMD at 273 K; **(e)** Energy evolution of AIMD at 1000 K.

Table 1 Second- and third-order elastic constants of $P2_12_12_1$-C16 (Unit: GPa).

Elastic constants	C_{11}	C_{12}	C_{13}	C_{22}	C_{23}	C_{33}	C_{44}	C_{55}	C_{66}	
C_{ij}	1065	66.5	69.4	1222	63.9	1056	498	406	511	
dC_{ij}/dP	6.07	1.19	0.63	6.07	0.83	5.86	2.24	1.31	2.32	
	C_{111}	C_{112}	C_{113}	C_{122}	C_{123}	C_{133}	C_{144}	C_{155}	C_{166}	C_{222}
C_{ijk}	–10176	–564	–146	–468	–497	–248	–273	–1367	–2468	–11261
	C_{223}	C_{233}	C_{244}	C_{255}	C_{266}	C_{333}	C_{344}	C_{355}	C_{366}	C_{456}
C_{ijk}	–103	–453	–1878	–338	–1956	–9853	–2374	–1537	–231	–557

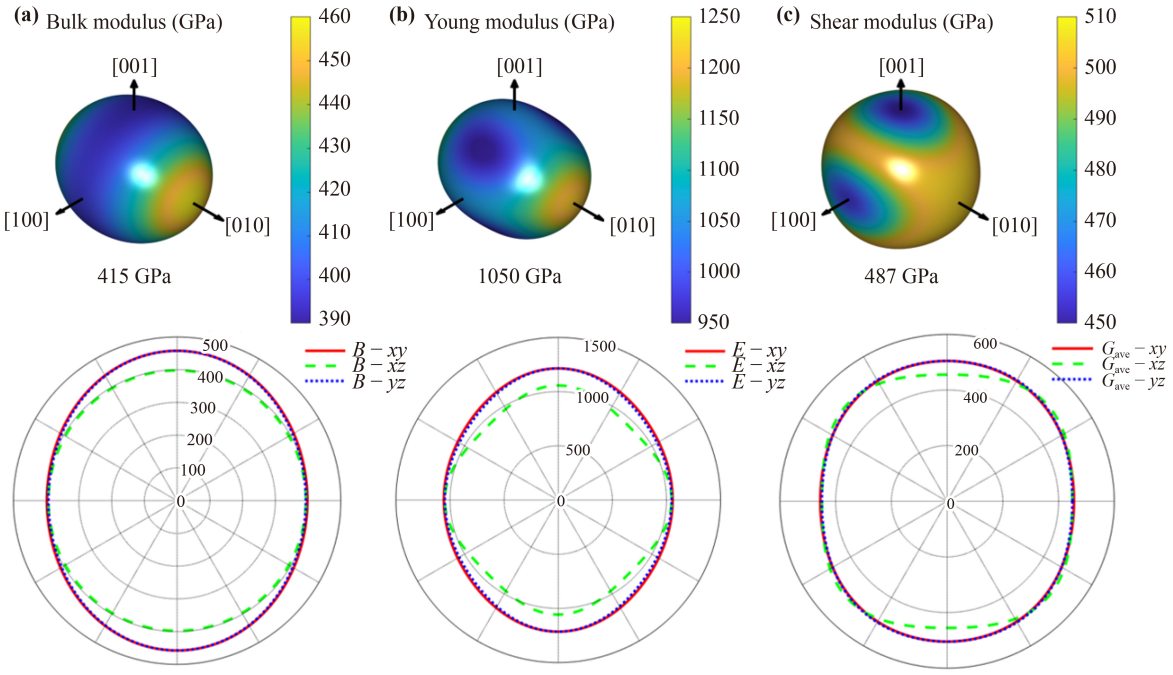

Fig. 4 Anisotropy of elastic modulus, unit in GPa. The number below each 3D figure is the averaged value by the VRH scheme. **(a)** Bulk modulus, B; **(b)** Young's modulus, E; **(c)** Shear modulus, G.

based model and Gao's model [40] confirm that $P2_12_12_1$-C16 is an ultrahard material.

Similar with the cubic system [57], using the TOECs, the derivatives of SOECs on pressure are calculated according to Ref. [58] (as Table 1). When compared with diamond [59], the dC_{11}/dP, dC_{22}/dP, dC_{33}/dP, dC_{44}/dP and dC_{66}/dP of $P2_12_12_1$-C16 are comparable with that of diamond, while the dC_{12}/dP, dC_{13}/dP, dC_{23}/dP and dC_{55}/dP of $P2_12_12_1$-C16 are obviously smaller than that of diamond.

3.4 Electronic and optical properties

The band structure of $P2_12_12_1$-C16 is illustrated in Fig. 5. The valence band top is at the Gamma point and the conduction band bottom is located between the Gamma point and the X point. The bandgap is 4.81 eV for PBE functional and 6.23 eV for HSE06 functional, and the direct bandgap is about 7.25 eV which is slightly larger than the known widest bandgap (7.24 eV) [21] of carbon allotropes. Hence, the BFOM of $P2_12_12_1$-C16 is about 2.6 times of diamond and 37.8 times of GaN [4]. When compared with other wide-bandgap carbon allotropes, as shown in Table 2, $P2_12_12_1$-C16 is comparable with tP12 and tri-C18, while $P2_12_12_1$-C16 is much stable than tP12 and more stable than tri-C18 at high pressure under which many new carbon allotropes

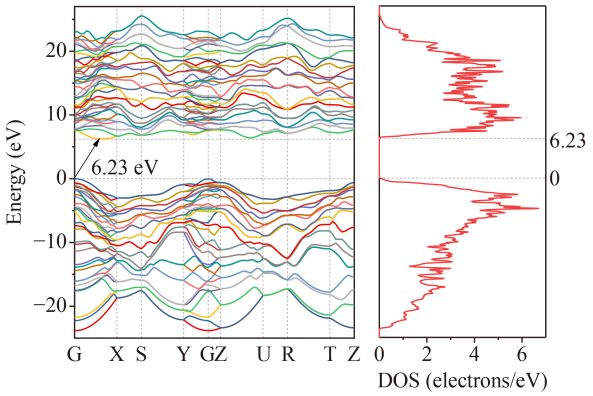

Fig. 5 Band structure of $P2_12_12_1$-C16 with HSE06.

Table 2 Bandgap of $P2_12_12_1$-C16 and compared with other large-bandgap carbon allotropes.

	E_g(PBE/LDA) (eV)	E_g (HSE06/PBE0) (eV)	Ref.
I-43d	5.91	7.24	[21]
Clathrate families	–	7.3(VIII), 6.9(II-100), 6.8(IV-100), 6.7(I-100), 6.6(VI)	[26][a]
I-4[23]	5.25	6.55	[21]
tri-C18	5.01	6.32	[20]
tP12 [22]	4.98, 5.4 [22]	6.27	[21]
$P2_12_12_1$-C16	**4.81**	**6.23**	**This work**
Pbam-32	4.76	5.97	[21]
O-carbon	4.54	5.87	[24]
W-carbon	4.39 [61]	5.69	[24]
BC14	–	5.64	[18]
C_{20}-T carbon	–	5.44	[62]
$P4_12_12_1$	4.70	–	[63]
Pbam-24	4.56, 4.57 [63]	–	[21]
Diamond	4.15 [21]	5.32 [21], 5.29 [20], 5.9 [23], 5.40 (This work)	5.47 (Exp) [15]

[a]Note: The bandgap is calculated with PBE0 functional in Karttunen's work [26], which obviously overestimates the bandgap.

are synthesized [60]. The wide-bandgap feature makes $P2_12_12_1$-C16 a promising material for high-temperature and high-efficiency applications if synthesized.

The optical properties are assessed by the dielectric function, and the refractive index (n) and absorption coefficient (κ) can be expressed as Eq.(1) [64]. Fig. 6 shows the dielectric function and refractive index of $P2_12_12_1$-C16 and compared to diamond. It is clear that the imaginary part of the dielectric function of $P2_12_12_1$-C16 is zero in the visible light area, which means that κ is zero according to Eq. (1). In other words, the single crystal of $P2_12_12_1$-C16 is transparent. The refractive index of $P2_12_12_1$-C16 is slightly higher than diamond, which indicates that $P2_12_12_1$-C16 will be more dazzling than diamond if synthesized,

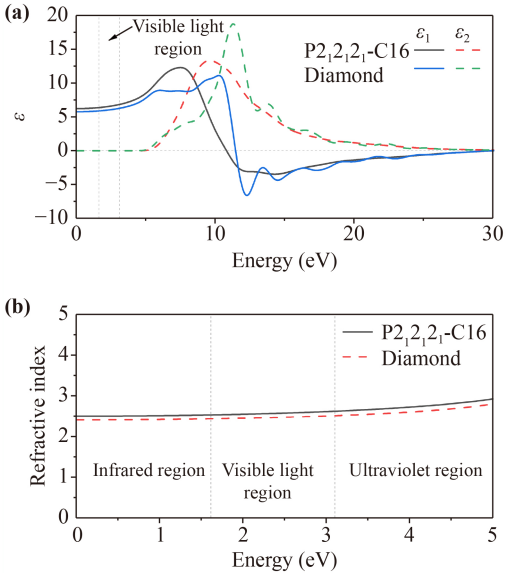

Fig. 6 Optical properties of $P2_12_12_1$-C16. **(a)** Dielectric function; **(b)** Refractive index.

$$\begin{cases} n = \sqrt{\left(\sqrt{\varepsilon_1^2+\varepsilon_2^2}+\varepsilon_1\right)/2} \\ \kappa = \sqrt{\left(\sqrt{\varepsilon_1^2+\varepsilon_2^2}-\varepsilon_1\right)/2} \end{cases}, \quad (1)$$

where ε_1 and ε_2 are the real and imaginary parts of the dielectric function.

3.5 Experimental possibility

To determine if $P2_12_12_1$-C16 can be synthesized from experiments, the XRD pattern of $P2_12_12_1$-C16 is simulated and compared with previous experiments[65, 66], as shown in Fig. 7. Clearly, the main peaks of $P2_12_12_1$-C16, including (101), (102), (200), (111), (112), (211), and (311), appear in the previous chimney soot [65], TNT/diesel soot [66] and shock-compressed carbon black and tetracyanoethylene powder mixture [67]. Though the peak at 29.3° can be indexed by several theoretical results, including Rh6 [51], Tri-C18 [20], and BCO-C16 [47], there are several peaks, such as 23.05°, 41.4°, and 77.15°, are only exists in $P2_12_12_1$-C16 and $P2_12_12_1$-C16 is more stable than Rh6, Tri-C18, and BCO-C16 at high pressure [Fig. 3(b)]. The good match between the simulated XRD and experiments indicates that $P2_12_12_1$-C16 is a good candidate for explaining the unknown phase in the experiments.

In addition, similar to M-carbon [68], W-carbon [61], H- and S-carbon [69], $P2_12_12_1$-C16 can be transformed from graphite. Figure 8 shows the hypothetically structural conversion paths. There are at least two transition pathways. In the first one (top in Fig. 8), there are four layers in the unit cell of $P2_12_12_1$-C16, and the layers are alternated by boat-1 and chair [70] configuration buckling from graphite sheet. The initial graphite sheet is AA stacking or AB stacking with a slide (as shown in the

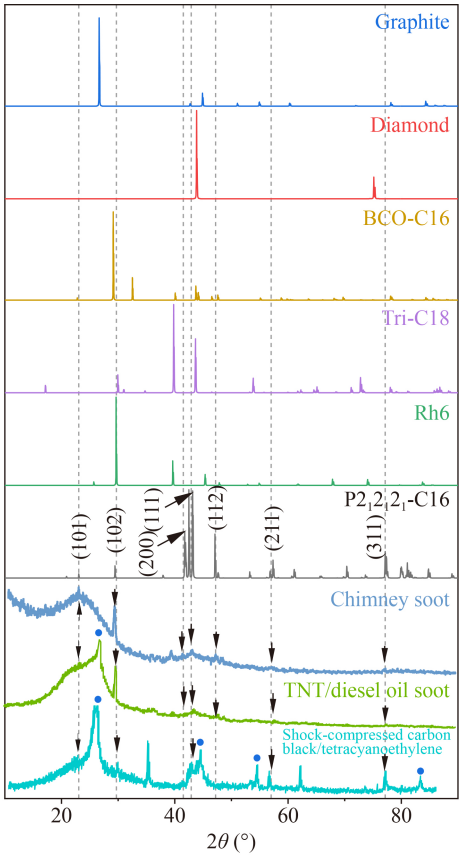

Fig. 7 Simulated XRD of $P2_12_12_1$-C16, diamond, and graphite and compared with experiments (Chimney soot sample in Ref. [65], soot of TNT/ diesel oil in water environment [66] and shock-compressed carbon black and tetracyanoethylene powder mixture [67]) and other theoretical results, including Rh6 [51], Tri-C18 [20] and BCO-C16 [47]. Cu target is taken as XRD source as the same in experiments. The black arrows (↓) show the peak of $P2_12_12_1$-C16, and the circle (•) are the peak of graphite.

left of Fig. 8). In the second pathway (right in Fig. 8), there are two layers in the unit cell, and each layer is composed of boat-1 (50%) and chair (50%) configuration. In this way, the $P2_12_12_1$-C16 can be formed by buckling and sliding from graphite (as shown in the bottom of Fig. 8). In both pathways, the layered characteristics indicate that the $P2_12_12_1$-C16 belongs to the superhard family proposed by Niu *et al.* [71] which can be synthesized via cold compression of graphite and nanotubes.

4 Conclusion

In conclusion, we have proposed a new ultrahard and ultrawide-bandgap orthorhombic all-sp^3 carbon allotrope ($P2_12_12_1$-C16) and made a comprehensive investigation of the structural stability, mechanical and electronic properties by first-principles calculations. The energy of $P2_12_12_1$-C16 is about 0.304 eV higher than that of diamond at 0 K and 0 Pa, which is lower than many

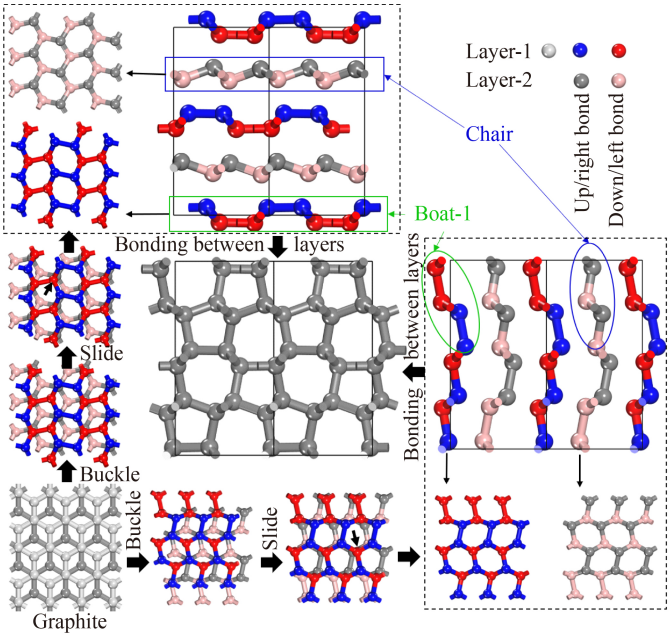

Fig. 8 Hypothetical transition pathway from graphite. In the layered picture, the pink/red and grey/blue balls correspond to carbon atoms with down (left) and up (right) bonds, respectively.

carbon allotropes, confirming the energetical stability. No imaginary frequency shown in the phonon spectrum validates the dynamic stability and the satisfaction of the Born criterion according to elastic constants proves the mechanical stability. The thermal stability at 273 K and 1000 K are confirmed by ab-initio molecular dynamics. The hardness is about 88 GPa to 93 GPa according to different models. The refractive index is larger than that of diamond in the visible light region, meaning that $P2_12_12_1$-C16 is more shining than diamond. The bandgap is about 6.23 eV by HSE06, which is larger than that of diamond about 0.91 eV. In addition, we proposed two hypothetical transition pathways from graphite to synthesize $P2_12_12_1$-C16 and the simulated XRD indicates the possible presence of $P2_12_12_1$-C16 in previous experiments.

Acknowledgements This work was supported by the National Natural Science Foundation of China (No. 51875269), and the Startup Foundation of Jiangsu University of Science and Technology (No. 202100000135).

References

1. J. Millan, P. Godignon, X. Perpina, A. Perez-Tomas, and J. Rebollo, A survey of wide bandgap power semiconductor devices, *IEEE Trans. Power Electron.* 29(5), 2155 (2014)
2. H. Okumura, A roadmap for future wide bandgap semiconductor power electronics, *MRS Bull.* 40(5), 439 (2015)

3. P. R. Wilson, B. Ferreira, J. Zhang, and C. DiMarino, IEEE ITRW: International technology roadmap for wide-bandgap power semiconductors: An overview, *IEEE Power Electron. Mag.* 5(2), 22 (2018)
4. J. Y. Tsao, S. Chowdhury, M. A. Hollis, D. Jena, N. M. Johnson, K. A. Jones, R. J. Kaplar, S. Rajan, C. G. Van de Walle, E. Bellotti, C. L. Chua, R. Collazo, M. E. Coltrin, J. A. Cooper, K. R. Evans, S. Graham, T. A. Grotjohn, E. R. Heller, M. Higashiwaki, M. S. Islam, P. W. Juodawlkis, M. A. Khan, A. D. Koehler, J. H. Leach, U. K. Mishra, R. J. Nemanich, R. C. N. Pilawa-Podgurski, J. B. Shealy, Z. Sitar, M. J. Tadjer, A. F. Witulski, M. Wraback, and J. A. Simmons, Ultrawide-bandgap semiconductors: Research opportunities and challenges, *Adv. Electron. Mater.* 4(1), 1600501 (2018)
5. B. J. Baliga, Semiconductors for high-voltage, vertical channel field-effect transistors, *J. Appl. Phys.* 53(3), 1759 (1982)
6. X. Shi, C. He, C. J. Pickard, C. Tang, and J. Zhong, Stochastic generation of complex crystal structures combining group and graph theory with application to carbon, *Phys. Rev. B* 97(1), 014104 (2018)
7. P. Gao, B. Gao, S. Lu, H. Liu, J. Lv, Y. Wang, and Y. Ma, Structure search of two-dimensional systems using CALYPSO methodology, *Front. Phys.* 17(2), 23203 (2022)
8. R.-S. Zhang and J.-W. Jiang, The art of designing carbon allotropes, *Front. Phys.* 14(1), 13401 (2019)
9. W. Tong, Q. Wei, H.-Y. Yan, M.-G. Zhang, and X.-M. Zhu, Accelerating inverse crystal structure prediction by machine learning: A case study of carbon allotropes, *Front. Phys.* 15(6), 63501 (2020)
10. H. W. Kroto, J. R. Heath, S. C. O'Brien, R. F. Curl, and R. E. Smalley, C_{60}: Buckminsterfullerene, *Nature* 318(6042), 162 (1985)
11. S. Iijima, Helical microtubules of graphitic carbon, *Nature* 354(6348), 56 (1991)
12. K. S. Novoselov, A. K. Geim, S. V. Morozov, D. Jiang, Y. Zhang, S. V. Dubonos, I. V. Grigorieva, and A. A. Firsov, Electric field effect in atomically thin carbon films, *Science* 306(5696), 666 (2004)
13. H. Tang, X. Yuan, Y. Cheng, H. Fei, F. Liu, T. Liang, Z. Zeng, T. Ishii, M.-S. Wang, T. Katsura, H. Sheng, and H. Gou, Synthesis of paracrystalline diamond, *Nature* 599(7886), 605 (2021)
14. X. -L. Sheng, Q. -B. Yan, F. Ye, Q. -R. Zheng, and G. Su, T-carbon: A novel carbon allotrope, *Phys. Rev. Lett.* 106(15), 155703 (2011)
15. F. Occelli, P. Loubeyre, and R. Letoullec, Properties of diamond under hydrostatic pressures up to 140 GPa, *Nat. Mater.* 2(3), 151 (2003)
16. X. -Y. Ding, C. Zhang, D. -Q. Wang, B. -S. Li, Q. Wang, Z. G. Yu, K. -W. Ang, and Y. -W. Zhang, A new carbon allotrope: T_5-carbon, *Scr. Mater.* 189, 72 (2020)
17. M. Liao, F. Wang, J. Zhu, Z. Lai, and Y. Liu, P2221-C8: A novel carbon allotrope denser than diamond, *Scr. Mater.* 212, 114549 (2022)
18. J. T. Wang, C. Chen, and H. Mizuseki, Body centered cubic carbon BC14: An all-sp^3 bonded full-fledged pentadiamond, *Phys. Rev. B* 102(18), 184106 (2020)
19. J. Liu, Q. Gao, and Z. Hu, HSH-carbon: A novel sp^2–sp^3 carbon allotrope with an ultrawide energy gap, *Front. Phys.* 17(6), 63505 (2022)
20. R. Lv, X. Yang, D. Yang, C. Niu, C. Zhao, J. Qin, J. Zang, F. Dong, L. Dong, and C. Shan, Computational prediction of a novel superhard sp^3 trigonal carbon allotrope with bandgap larger than diamond, *Chin. Phys. Lett.* 38(7), 076101 (2021)
21. C. He, X. Shi, S. J. Clark, J. Li, C. J. Pickard, T. Ouyang, C. Zhang, C. Tang, and J. Zhong, Complex low energy tetrahedral polymorphs of group IV elements from first principles, *Phys. Rev. Lett.* 121(17), 175701 (2018)
22. Q. Zhu, A. R. Oganov, M. A. Salvadó, P. Pertierra, and A. O. Lyakhov, Denser than diamond: *Ab initio* search for superdense carbon allotropes, *Phys. Rev. B* 83(19), 193410 (2011)
23. X. Zhang, Y. Wang, J. Lv, C. Zhu, Q. Li, M. Zhang, Q. Li, and Y. Ma, First-principles structural design of superhard materials, *J. Chem. Phys.* 138(11), 114101 (2013)
24. J. Wang, C. Chen, and Y. Kawazoe, Orthorhombic carbon allotrope of compressed graphite: *Ab initio* calculations, *Phys. Rev. B* 85(3), 033410 (2012)
25. C. J. Pickard and R. J. Needs, *Ab initio* random structure searching, *J. Phys.: Condens. Matter* 23(5), 053201 (2011)
26. A. J. Karttunen, T. F. Fässler, M. Linnolahti, and T. A. Pakkanen, Structural principles of semiconducting group 14 clathrate frameworks, *Inorg. Chem.* 50(5), 1733 (2011)
27. H. Yin, X. Shi, C. He, M. Martinez-Canales, J. Li, C. J. Pickard, C. Tang, T. Ouyang, C. Zhang, and J. Zhong, Stone–Wales graphene: A two-dimensional carbon semimetal with magic stability, *Phys. Rev. B* 99(4), 041405 (2019)
28. S. J. Clark, M. D. Segall, C. J. Pickard, P. J. Hasnip, M. I. J. Probert, K. Refson, and M. C. Payne, First principles methods using CASTEP, *Z. Kristallogr.* 220, 567 (2005)
29. J. E. Peralta, J. Heyd, G. E. Scuseria, and R. L. Martin, Spin–orbit splittings and energy band gaps calculated with the Heyd–Scuseria–Ernzerhof screened hybrid functional, *Phys. Rev. B* 74(7), 073101 (2006)
30. J. P. Perdew, K. Burke, and M. Ernzerhof, Generalized gradient approximation made simple, *Phys. Rev. Lett.* 77(18), 3865 (1996)
31. D. R. Hamann, M. Schlüter, and C. Chiang, Norm-conserving pseudopotentials, *Phys. Rev. Lett.* 43(20), 1494 (1979)
32. D. Vanderbilt, Soft self-consistent pseudopotentials in a generalized eigenvalue formalism, *Phys. Rev. B* 41(11), 7892 (1990)
33. B. G. Pfrommer, M. Côté, S. G. Louie and M. L. Cohen, Relaxation of crystals with the quasi-Newton method, *J. Comput. Phys.* 131(1), 233 (1997)
34. S. Baroni, S. de Gironcoli, A. Dal Corso, and P. Giannozzi, Phonons and related crystal properties from density-functional perturbation theory, *Rev. Mod. Phys.* 73(2), 515 (2001)
35. M. Liao, Y. Liu, F. Zhou, T. Han, D. Yang, N. Qu, and Z. Lai, A high-efficient strain-stress method for calculating higher-order elastic constants from first-principles, *Comput. Phys. Commun.* 280, 108478 (2022)
36. M. Liao, Y. Liu, S.-L. Shang, F. Zhou, N. Qu, Y. Chen, Z. Lai, Z.-K. Liu, and J. Zhu, Elastic3rd: A tool for

calculating third-order elastic constants from first-principles calculations, *Comput. Phys. Commun.* 261, 107777 (2021)
37. M. Liao, Y. Liu, Y. Wang, F. Zhou, N. Qu, T. Han, D. Yang, Z. Lai, Z.-K. Liu, and J. Zhu, Revisiting the third-order elastic constants of diamond: The higher-order effect, *Diam. Relat. Mater.* 117, 108490 (2021)
38. R. Hill, The elastic behaviour of a crystalline aggregate, *Proc. Phys. Soc. Sect. A* 65(5), 349 (1952)
39. M. Liao, Y. Liu, P. Cui, N. Qu, F. Zhou, D. Yang, T. Han, Z. Lai, and J. Zhu, Modeling of alloying effect on elastic properties in BCC Nb–Ti–V–Zr solid solution: From unary to quaternary, *Comput. Mater. Sci.* 172, 109289 (2020)
40. F. Gao, J. He, E. Wu, S. Liu, D. Yu, D. Li, S. Zhang, and Y. Tian, Hardness of covalent crystals, *Phys. Rev. Lett.* 91(1), 015502 (2003)
41. V. A. Blatov, A. P. Shevchenko, and D. M. Proserpio, Applied topological analysis of crystal structures with the program package topospro, *Cryst. Growth Des.* 14(7), 3576 (2014)
42. V. A. Blatov, O. A. Blatova, F. Daeyaert, and M. W. Deem, Nanoporous materials with predicted zeolite topologies, *RSC Adv.* 10(30), 17760 (2020)
43. R. Hoffmann, A. A. Kabanov, A. A. Golov, and D. M. Proserpio, Homo citans and carbon allotropes: For an ethics of citation, *Angew. Chemie Int. Ed.* 55(37), 10962 (2016)
44. M. Al-Fahdi, A. Rodriguez, T. Ouyang, and M. Hu, High-throughput computation of new carbon allotropes with diverse hybridization and ultrahigh hardness, *Crystals* 11(7), 783 (2021)
45. N. A. Anurova, V. A. Blatov, G. D. Ilyushin, and D. M. Proserpio, Natural tilings for zeolite-type frameworks, *J. Phys. Chem. C* 114(22), 10160 (2010)
46. O. Delgado-Friedrichs and M. O'Keeffe, Identification of and symmetry computation for crystal nets, *Acta Crystallogr. Sect. A Found. Crystallogr.* 59(4), 351 (2003)
47. J.-T. Wang, H. Weng, S. Nie, Z. Fang, Y. Kawazoe, and C. Chen, Body-centered orthorhombic C_{16}: A novel topological node-line semimetal, *Phys. Rev. Lett.* 116(19), 195501 (2016)
48. N. N. Matyushenko, V. E. Strel'Nitskiĭ, and V. A. Gusev, A dense new version of crystalline carbon C_8, *JETP Lett.* 30(4), 199 (1979)
49. R. L. Johnston and R. Hoffmann, Superdense carbon, C_8: supercubane or analog of . gamma. -silicon? *J. Am. Chem. Soc.* 111(3), 810 (1989)
50. Z.-Z. Li, C.-S. Lian, J. Xu, L.-F. Xu, J.-T. Wang, and C. Chen, Computational prediction of body-centered cubic carbon in an all-sp^3 six-member ring configuration, *Phys. Rev. B* 91(21), 214106 (2015)
51. J. -T. Wang, C. Chen, E. Wang, and Y. Kawazoe, A new carbon allotrope with six-fold helical chains in all-sp^2 bonding networks, *Sci. Rep.* 4(1), 4339 (2015)
52. F. Mouhat and F.-X. Coudert, Necessary and sufficient elastic stability conditions in various crystal systems, *Phys. Rev. B* 90(22), 224104 (2014)
53. S. F. Pugh, XCII. Relations between the elastic moduli and the plastic properties of polycrystalline pure metals, *London, Edinburgh, Dublin Philos. Mag. J. Sci.* 45(367), 823 (1954)
54. X. Chen, H. Niu, D. Li, and Y. Li, Modeling hardness of polycrystalline materials and bulk metallic glasses, *Intermetallics* 19(9), 1275 (2011)
55. Y. Tian, B. Xu, and Z. Zhao, Microscopic theory of hardness and design of novel superhard crystals, *Int. J. Refract. Met. Hard Mater.* 33, 93 (2012)
56. E. Mazhnik and A. R. Oganov, A model of hardness and fracture toughness of solids, *J. Appl. Phys.* 126(12), 125109 (2019)
57. M. Liao, Y. Liu, Z. Lai, and J. Zhu, Pressure and temperature dependence of second-order elastic constants from third-order elastic constants in TMC (TM=Nb, Ti, V, Zr), *Ceram. Int.* 47(19), 27535 (2021)
58. R. R. Rao and A. Padmaja, Effective second-order elastic constants of a strained crystal using the finite strain elasticity theory, *J. Appl. Phys.* 62(2), 440 (1987)
59. H. J. McSkimin and P. Andreatch, Elastic moduli of diamond as a function of pressure and temperature, *J. Appl. Phys.* 43(7), 2944 (1972)
60. B. Sundqvist, Carbon under pressure, *Phys. Rep.* 909, 1 (2021)
61. J. Wang, C. Chen, and Y. Kawazoe, Low-temperature phase transformation from graphite to sp^3 orthorhombic carbon, *Phys. Rev. Lett.* 106(7), 075501 (2011)
62. J. Q. Wang, C. X. Zhao, C. Y. Niu, Q. Sun, and Y. Jia, C_{20}-T carbon: A novel superhard sp^3 carbon allotrope with large cavities, *J. Phys.: Condens. Matter* 28(47), 475402 (2016)
63. A. Mujica, C. J. Pickard and R. J. Needs, Low-energy tetrahedral polymorphs of carbon, silicon, and germanium, *Phys. Rev. B* 91(21), 214104 (2015)
64. L. D. Landau and E. M. Lifshitz, in: Electrodynamics of Continuous Media (2nd Ed.), Eds. L. D. Landau and E. M. Lifshitz, Pergamon, Amsterdam, Second Edi. (1984), Vol. 8, pp 257–289
65. D. Pantea, S. Brochu, S. Thiboutot, G. Ampleman, and G. Scholz, A morphological investigation of soot produced by the detonation of munitions, *Chemosphere* 65(5), 821 (2006)
66. P. Chen, F. Huang, and S. Yun, Characterization of the condensed carbon in detonation soot, *Carbon* 41(11), 2093 (2003)
67. K. Yamada, Shock synthesis of a new cubic form of carbon, *Carbon* 41(6), 1309 (2003)
68. Q. Li, Y. Ma, A. R. Oganov, H. Wang, H. Wang, Y. Xu, T. Cui, H.-K. Mao, and G. Zou, Superhard monoclinic polymorph of carbon, *Phys. Rev. Lett.* 102(17), 175506 (2009)
69. C. He, L. Sun, C. Zhang, X. Peng, K. Zhang, and J. Zhong, New superhard carbon phases between graphite and diamond, *Solid State Commun.* 152(16), 1560 (2012)
70. C. He, C. X. Zhang, L. Z. Sun, N. Jiao, K. W. Zhang, and J. Zhong, Structure, stability and electronic properties of tricycle type graphane, *Phys. Status Solidi - Rapid Res. Lett.* 6(11), 427 (2012)
71. H. Niu, X.-Q. Chen, S. Wang, D. Li, W. L. Mao, and Y. Li, Families of superhard crystalline carbon allotropes constructed via cold compression of graphite and nanotubes, *Phys. Rev. Lett.* 108(13), 135501 (2012)